HHS Public Access

Author manuscript

Stem Cell Res. Author manuscript; available in PMC 2022 August 11.

Published in final edited form as:

Stem Cell Res. 2021 August ; 55: 102496. doi:10.1016/j.scr.2021.102496.

Chromatin accessibility profiling identifies evolutionary conserved loci in activated human satellite cells

Lisa S. Chow[a], **Darko Bosnakovski**[b,c,d], **Douglas G. Mashek**[a,e], **Michael Kyba**[b,c,g], **Rita C. R. Perlingeiro**[b,f,g], **Alessandro Magli**[b,f,g,*]

[a]Division of Diabetes, Endocrinology and Metabolism, Department of Medicine, University of Minnesota, Minneapolis, MN, USA

[b]Lillehei Heart Institute, University of Minnesota, Minneapolis, MN, USA

[c]Department of Pediatrics, University of Minnesota, Minneapolis, MN, USA

[d]University Goce Delcev - Shtip, Faculty of Medical Sciences, Shtip, Macedonia

[e]Department of Biochemistry, Molecular Biology, and Biophysics, University of Minnesota, Minneapolis, MN, USA

[f]Division of Cardiology, Department of Medicine, University of Minnesota, Minneapolis, MN USA

[g]Stem Cell Institute, University of Minnesota, Minneapolis, MN, USA

Abstract

Satellite cells represent the main myogenic population accounting for skeletal muscle homeostasis and regeneration. While our knowledge of the signaling pathways controlling satellite cell regenerative capability is increasing, the underlying epigenetic mechanisms are still not clear, especially in the case of human satellite cells. Here, by performing chromatin accessibility profiling (ATAC-seq) in samples isolated from human and murine muscles, we investigated the changes in the epigenetic landscape occurring during the transition from activated satellite cells to myoblasts. Our analysis identifies a compendium of putative regulatory elements defining human activated satellite cells and myoblasts, respectively. A subset of these differentially accessible loci is shared by both murine and human satellite cells, includes elements associated with known self-renewal regulators, and is enriched for motifs bound by transcription factors participating in satellite cell regulation. Integration of transcriptional and epigenetic data reveals that known

*Corresponding author at: Lillehei Heart Institute, University of Minnesota, 4-130 CCRB, 2231 6th St. SE, Minneapolis, MN 55455, USA. amagli@umn.edu (A. Magli).

CRediT authorship contribution statement

Lisa S. Chow: Resources, Writing - review & editing, Funding acquisition. **Darko Bosnakovski:** Methodology. **Douglas G. Mashek:** Resources. **Michael Kyba:** Resources, Writing - review & editing. **Rita C.R. Perlingeiro:** Resources, Writing - review & editing. **Alessandro Magli:** Conceptualization, Data curation, Formal analysis, Funding acquisition, Investigation, Methodology, Project administration, Supervision, Validation, Visualization, Writing – original draft, Writing - review & editing.

Declaration of Competing Interest

The authors declare that they have no known competing financial interests or personal relationships that could have appeared to influence the work reported in this paper.

Appendix A. Supplementary data

Supplementary data to this article can be found online at https://doi.org/10.1016/j.scr.2021.102496.

regulators of metabolic gene expression, such as PPARGC1A, represent potential PAX7 targets. Through characterization of genomic networks and the underlying effectors, our data represent an important starting point for decoding and manipulating the molecular mechanisms underlying human satellite cell muscle regenerative potential.

Keywords

Human satellite cell; Muscle stem cell; ATAC-seq; Regulatory element; Pax7; PGC1 alpha

1. Introduction

Skeletal muscle accounts for approximately 40% of the human body weight. Since skeletal muscle participates in many processes including locomotion, respiration and body metabolism, its maintenance is fundamental for healthy lifespan. Adult muscle homeostasis is ensured by satellite cells, a stem cell population capable of generating transient proliferating progenitors (myoblasts) that will ultimately differentiate and integrate into fibers to repair damage, or fuse to generate fibers de novo (reviewed by (Feige et al., 2018). In both human and mouse, these cells are marked by Pax7 expression (Reimann et al., 2004; Seale et al., 2000) and are located beneath the muscle basal lamina in a quiescent state (Feige et al., 2018). The intrinsic regenerative capability of satellite cells makes this population the ideal candidate for muscle cell therapy. Yet, satellite cells are unable to self-renew outside of their physiological context and in vitro culture results in loss of their stem cell properties (Montarras et al., 2005; Sacco et al., 2008). To enable the use of satellite cells for regenerative medicine applications, it is critical to decode the mechanisms governing the balance between quiescence/self-renewal and activation/proliferation.

Since the identification of Pax7 as a satellite cell marker, multiple groups have contributed to the understanding of the mechanisms regulating muscle stem cell maintenance and myogenic progression (Feige et al., 2018). Nonetheless, while it became clear that satellite cell function is controlled at multiple levels, only few studies have investigated the genomic elements regulating gene expression in this stem cell population. Profiling of H3K4me and H3K27me3 in mouse satellite cells identified potential epigenetic determinants underlying the functional decline in stem cell quiescence during aging (Liu et al., 2013) and, in agreement with this finding, aged murine satellite cells display increased chromatin accessibility at facultative heterochromatin sites (Shcherbina et al., 2020). Ryall and colleagues found that H4K16Ac levels increase at myogenic promoters following murine satellite cell in vitro expansion, and demonstrated that the histone deacetylase Sirt1 prevents the deposition of this mark in satellite cells (Ryall et al., 2015). Interestingly, more recent studies showed that changes in genomic distribution of H3K27Ac and H3K4me3 occur as early as 3 h from their dissociation from the muscle fiber (Machado et al., 2017), demonstrating that satellite cells quickly transit from the quiescent to the activated state (Machado et al., 2017; van Velthoven et al., 2017). As precision medicine technologies become more accessible, we believe that a comprehensive understanding of satellite cell epigenetic regulation will be instrumental for manipulating regenerative capacity of these cells.

Although these studies are relevant for identifying regulatory elements underlying murine satellite cell quiescence and activation, no such data are yet available for human satellite cells. Scarce access to human specimens and technological limitations associated with traditional chromatin immunoprecipitation analyses (e.g. H3K27Ac ChIP-seq) have so far proven to be major barriers. To address this gap, we used ATAC-seq (Assay for Transposase-Accessible Chromatin followed by sequencing, (Buenrostro et al., 2013) to generate maps of chromatin accessibility in freshly-isolated human satellite cells and myoblasts. Chromatin accessibility correlates with transcription factor binding and nucleosome occupancy, thus providing important information about the epigenetic status of gene promoters and transcriptional enhancers (Shlyueva et al., 2014). Moreover, in contrast to traditional ChIP-seq protocols, ATAC-seq can be easily performed with<50,000 cells, thus enabling epigenetic studies in rare populations (Buenrostro et al., 2015). Following integration of the chromatin accessibility landscape with available transcriptomic data as well as comparable datasets generated using murine satellite cells and myoblasts, our studies identify a compendium of putative conserved regulatory elements controlling gene expression in activated satellite cells and myoblasts. Functional classification of these loci evidenced that a subset of regulators of metabolic gene expression may represent novel PAX7 targets. Altogether, our data identify potential regulatory elements underlying human satellite cell function.

2. Material and methods

2.1. Human biopsies

De-identified human muscle biopsies were obtained from healthy subjects (details provided in Table 1). This study was approved by the University of Minnesota Institutional Review Board (STUDY00002730) and conducted in accordance with the Declaration of Helsinki. All participants provided written informed consent before participation. All biopsies were performed in the fasting state. Muscle biopsies were collected using a Bergstrom needle (6.35 mm) inserted into the vastus lateralis muscle followed by suction. Tissue was then transferred into a 15 ml conical tube filled with Ham's/F-10 media and immediately processed for satellite cell isolation.

2.2. Animals

Animal experiments were carried out according to protocols approved by the University of Minnesota Institutional Animal Care and Use Committee. *Pax7-ZsGreen* mice (Bosnakovski et al., 2008) maintained in the C57BL/6 background were used for satellite cell isolation.

2.3. Satellite cell isolation and flow cytometry

Human and murine satellite cells were isolated from the muscle mononuclear fraction obtained following tissue enzymatic digestion. More specifically, dissected muscles or sample biopsies were minced into fragments of 1–3 mm size using a razor blade, transferred into a conical tube and incubated with a Collagenase II digestion solution (2 mg/ml Collagenase II in DMEM high glucose and 1% penicillin/streptomycin) for 75 min (60 min for human tissue) at 37 °C in a shaker set at 200 rpm. Human biopsies (between 50 and 100 mg) were incubated with 3 ml of digestion solution in a 15 ml tube; for murine tissues,

15 ml of digestion solution were used to digest the muscles dissected from one hindlimb (using a 50 ml tube). After digestion, tubes were then centrifuged at 1000g for 7 min at 4 °C and, after aspirating the top 50% of the digestion solution, the remaining was washed with 2 volumes of Rinsing Solution (10% Horse Serum (Hyclone), 1% Penicillin/Streptomycin and 0.1 μM HEPES in Ham's/F-10 media - Hyclone) and then centrifuged at 1000g for 7 min at 4 °C, repeating this procedure twice. After the second wash, the pellet was further shredded with the help of a glass pipette (resuspending 5–7 times) and centrifuged at 1000g for 7 min at 4 °C. The resulting supernatant was carefully aspirated (leaving approximately 3–4 mm of volume above to not disturb the pellet), resuspended in a Dispase-Collagenase II digestion solution (0.1 mg/ml collagenase II and 0.5 mg/ml dispase in rinsing solution), vortexed for 20 s and incubated 30 min (20 min for human tissue) at 37 °C in a shaker set at 200 rpm. Following the second digestion, tubes were vortexed for 20 s and then further homogenized using a syringe equipped with a 16 gauge (G) followed by 18 G needle. The homogenate was then filtered through a 40 μm filter and then centrifuged at 1000g for 7 min at 4 °C. Before centrifuge, the tube used for the digestion was washed twice using 3 ml of rinsing solution and each wash was applied to the 40 μm filter, thus combining it to the original homogenate volume. After carefully aspirating the supernatant, the resulting pellet represented the mononuclear muscle fraction. In general, due to the small size of the biopsy, human samples were devoid of red cells. If necessary, cell pellets were incubated with ACK lysis buffer (Thermoscientific) following the manufacturers' instructions. Human samples were resuspended in 1 ml of MACS buffer supplemented with 10 μl of human Fc-Block (Miltenyi Biotec), incubated 5 min on ice and then supplemented with 10 μl of PE-conjugated anti-CD82 (clone ASL-24 – Biolegend) and 10 μl of APC-conjugated anti-CD56 (clone 5.1H11 – Biolegend) followed by a 30-minute incubation on ice. Cells were washed with 10 ml of sterile PBS, centrifuged for 7 min at 4 °C and resuspended in 1 ml of MACS buffer (Miltenyi Biotec) supplemented with Propidium Iodide (PI). Human satellite cells were identified as CD56 + CD82 + . Sorted human cells were collected in human myoblast culture media (described below). Murine samples were obtained from 8 to 12 week old Pax7-ZsGreen reporter mice. In this case, cell pellets were resuspended in MACS buffer supplemented with PI (4 ml for each hindlimb-derived fraction) and then processed for FACS. Murine satellite cells were identified as ZsGreen + . Sorted murine cells were collected in murine myoblast culture media (described below). All cell sorting experiments were performed using a FACS AriaII instrument (BD Biosciences). For data visualization, flow cytometry data (fcs files) were re-analyzed using FlowJo.

2.4. Cell culture, lentiviral transduction, immunostaining and RNA analysis

Sorted human and murine satellite cells were plated onto 0.1% gelatin coated plates maintained in a humidified incubator at 37 °C, 5% CO2, 5% O2. 500–1000 human satellite cells were plated in a 24-well plate following each isolation. Human cells were cultured using human myoblast culture media: Ham's/F-10 media (Hyclone) supplemented with 20% FBS (Sigma Aldrich), 1% penicillin/streptomycin (Thermoscientific), 500 nM dexamethasone (Cayman Chemical), 2 ng/ml basic fibroblast growth factor (Peprotech), 143 μM β-mercaptoethanol (Sigma Aldrich). Murine satellite cells were cultured using murine myoblast culture media: DMEM/F12 medium (Thermoscientific) supplemented with 20% FBS, 5 ng/ml basic fibroblast growth factor, 1% penicillin/streptomycin, and

0.25% chick embryonic extract (US Biological). All cells were sub-cultured when density reached 40–50%. For terminal myogenic differentiation, human cells were plated in 24-well plate and allowed to reach 90–100% density. Confluent cultures were washed once with PBS and switched to differentiation media: DMEM low glucose (Thermoscientific) supplemented with 5% Horse Serum (Sigma Aldrich), 1% penicillin/streptomycin, 1% Glutamax (Thermoscientific). 30–36 h later, cells were fixed using 4% paraformaldehyde (in PBS) for 10 min at 4 °C and processed for immunostaining. For PAX7 analysis, 10 µl of freshly sorted cells were plated on a Superfrost Plus microscope slide (Fisher Scientific), allowed to quickly dry in a 37 °C incubator, fixed with 4% paraformaldehyde and processed for immunostaining.

Briefly, cells were permeabilized 10 min at room temperature (RT) using 0.3% TRITON X-100 in PBS, washed once with PBS and incubated 30 min in blocking solution (5% Bovine Serum Albumin in PBS) at RT. Cells were incubated overnight at 4 °C with primary antibodies diluted (1:20) in blocking solution. Antibody used: anti-myosin heavy chain (clone MF20) and anti-PAX7 (clone PAX7), both from Developmental Studies Hybridoma Bank. Cells were washed twice with PBS, once with blocking solution, and incubated 1 h at RT with Alexa555-cojugated anti-mouse antibody (Thermoscientific) diluted (1:400) + DAPI in blocking solution. Cells were washed 3 times with PBS and then imaged using an Axio Imager M2 (for slides) or an Axio Observer Z1 (for 24-well plate) fluorescent microscope (both from Zeiss).

Lentiviral particles were generated by transfecting HEK 293 T cells (growing in 6 cm dishes) using the following plasmids: pVSV-G, pΔ8.9 and pRRL-PGK-GFP (control vector – Addgene plasmid #12252) and pRRL-PGK-Pax7 (mouse Pax7-expressing vector). Cloning details for the Pax7 construct are available upon request. Cell supernatants for each virus were collected 36–50-hour post transfection, passed through a 0.45 µm filter and combined. Lentiviral transductions were performed by plating 7,000 ZsGreen + cells onto 6-well plates. 24 h later, cells were supplemented with the supernatant containing the lentiviral particles in presence of 5 µg/ml polybrene and centrifuged at 1100g for 90 min, 30 °C. 4-hour post transduction, media was replaced with fresh one and cells were cultured for 4 days as described above. Cells were collected for RNA analysis using Trizol. Total RNAs were isolated following manufacturers' instructions. First strand cDNA synthesis was performed using Superscript RT Vilo (Thermoscientific). Quantitative PCR was performed on an Applied Biosystems™ QuantStudio™ 6 Flex Real-Time PCR System using TaqMan probes (Thermoscientific).

2.5. ATAC-seq

2.5.1. Library generation—Chromatin accessibility studies were performed following the protocol described by Buenrostro and colleagues (Buenrostro et al., 2015). Except for freshly isolated human cells, which isolation yield ranged between 5,000 and 10,000 cells, all other samples consisted of 50,000 cells (freshly sorted mouse cells, cultured mouse and human cells). Briefly, cells were washed with 200 µl of cold PBS then resuspended in 100 µl of cold lysis buffer (10 mM Tris-HCl pH 7.4, 10 mM NaCl, 3 mM MgCl2, 0.1% IGEPAL CA-630), spun at 500 g for 10 min at 4 °C and resuspended in 50 µl of the transposition

reaction mix. Transposition occurred at 37 °C for 30 min, after which transposed DNA was purified using a Qiagen MinElute Kit and eluted in 10 μl Elution Buffer. PCR amplification using Illumina-compatible adapter-barcodes and final library preparation were performed at the University of Minnesota Genomic Center. After Quality Control, libraries were pooled and sequenced on Paired-End runs of the HiSeq2500 operated at High Output mode (Illumina). Sequencing statistics are provided in Table S1.

2.5.2. Mapping—Reads were then mapped to the human (hg38) or mouse (mm10) genome using Bowtie2 (parameters -I 38 -X 2000 –local –dovetail -–no-mixed -–no-discordant) and filtered to remove mitochondrial reads and PCR duplicates. Peaks were identified using MACS2.1.1 (parameters –nomodel –nolambda –keep-dup all –call-summits -q 0.05 -B) and, for easier visualization, the resulting bedGraph files were converted to the BigWig format using Kent tools. Mapping and peak calling was also performed using the ENCODE ATAC-seq pipeline (summary output reported in Table S1).

2.5.3. Differential analysis—Analysis of differential accessibility (Figs. 1 and 3) was performed by generating a list of peaks representative of all samples using the peak summits identified by MACS2. Each summit was extended 50 bp in both directions and the resulting lists of peaks were combined, sorted and merged to obtain a dataset of unique and non-overlapping loci. Analysis of chromatin accessibility at human and murine promoters (Fig. 1 and S4) was performed using the 500 bp region upstream of each annotated TSS (from the hg38 and mm10 refGene – UCSC genome). The list of loci used for comparing human satellite cell and ENCODE data (Fig. 2) was generated using the coordinates retrieved from the narrowPeak files produced by MACS2. Only tissues with at least 2 available ATAC-seq datasets were considered for this analysis. The peak coordinates for all samples were combined, sorted and merged to obtain a dataset of unique and non-overlapping loci. For each differential analysis, the respective list was then used to extrapolate the sequencing depth coverage from each sample bedGraph file using Bedtools map. Coverage files were then analyzed using DEseq2 to identify loci with differential chromatin accessibility. Loci in human and murine activated satellite cells vs cultured cells (Fig. 1A and 3A, respectively) were selected based on q-value < 0.01 (False Discovery Rate) and absolute log2FoldChange > 3. Differentially accessible promoters in human and murine datasets (Fig. S2D and S4D, respectively) were selected based on q-value < 0.05. Comparison of human activated satellite cells, 12-day myoblasts and ENCODE data (Fig. 2A) was performed using q-value < 0.001 and absolute log2FoldChange > 4 & baseMean > 300. Heatmaps and clusters were created using R v3.6.3 and the pheatmap package from combined coverage data via a custom R script. Heatmaps show scaled (Z score) coverage information for each region in the relevant peak list file. Clusters in Fig. 2 were generated using the distance measurements from pheatmap and the R function cutree to get a specified number of clusters equal to 15.

2.5.4. Peak list comparisons—List of peaks in the Bed format were compared using Bedtools intersect. Human loci associated with differential chromatin accessibility (Fig 1A - Group 1 and 2) were compared to the list of CTCF ChIP-seq peaks from human myoblasts (ENCFF586KHT and ENCFF741PXH). Murine loci associated with differential chromatin accessibility (Fig. 3A - Group 1 and 2; Fig. 3C – Cluster A, B, C and D) were compared

to Pax7 ChIP-seq peaks identified in ES-derived myogenic progenitors. The latter list was generated using MACS2.1.1 (parameters: –keep-dup all –call-summits -q 0.01) followed by removal of the mouse blacklist peaks. To identify synthenic chromatin accessible loci, genomic coordinates corresponding to human Group 1 and 2 loci (Fig. 1A) were converted to the equivalent murine (mm10) genomic positions using the liftOver tool available at the UCSC website.

2.5.5. Motif analysis—Motif analysis was performed using the MEME suite 5.2.0 (default parameters). For these analyses, peak summits for Group 1 and 2 loci (both Fig. 1A and Fig. 3A) were extended of 100 bp in both directions (total 200 bp). Peak summits for conserved human-mouse loci (Fig. 4A) were extended of 250 bp in both directions (total 500 bp). Footprint analysis for the TFs in Fig. 4D at murine-human conserved loci was performed using RGT-HINT (Li et al., 2019) with the options –atac-seq and –paired-end. Table S5 reports position and score computed by the RGT-HINT pipeline.

2.6. ChIP-seq

Sequencing data were mapped to the murine (mm10) genome using Bowtie2 (–local) and then filtered to remove mitochondrial reads and PCR duplicates. Peak calling was performed using QESEQ (parameters -s 100 -c 15 -p 0.01) and the resulting enrichment files (.enr.sgr) were used for generating the k-means clustering map (Fig. 3C) with SeqMiner.

2.7. RNA-seq

2.7.1. Mapping and analysis—Human transcriptomic data were mapped to the human reference genome (hg38). Data were analyzed using the CHURP pipeline. Differentially expressed transcripts were identified using DESeq2, considering differentially expressed all transcripts with $q < 0.05$ and absolute log2FoldChange > 2. For visualization using IGV, mapped files (.bam) were converted to the BigWig format. Data representing the differential transcriptomic analyses “quiescent-vs-activated” and “activated-vs-cultured” for murine satellite cells were retrieved from the supplementary material of the corresponding manuscripts (Ryall et al., 2015; Machado et al., 2017; van Velthoven et al., 2017).

2.7.2. Functional annotation—Peaks from differentially chromatin accessibility analyses were annotated using GREAT (http://bejerano.stanford.edu/great/public/html/). GREAT association rules Fig. S2C, S3A and S4C: basal + extension: 5000 bp upstream, 1000 bp downstream, 500 kb max extension, curated regulatory domains included. GREAT association rule Fig. 5A: Two nearest genes: 500 kb, curated regulatory domains included. The list of genes displaying differential chromatin accessibility at the promoter level (Fig S2D and S4D) was compared to the list of differentially expressed transcripts (maintaining expression log2 fold change) and then imported into Ingenuity Pathway Analysis Software (Qiagen) for identification of canonical pathways, upstream regulators and their targets.

2.8. Statistical analyses

Identification of differential chromatin accessible loci and differentially expressed genes was performed using an adjusted p-value (False Discovery rate) < 0.01. Comparison of gene expression fold change between promoters (Fig. 1E) was performed using one-way ANOVA.

Satellite cell-specific loci identification (from comparison with ENCODE data – Fig. 2A) was performed using an adjusted p-value < 0.0001. Statistical analyses between control and Pax7-transduced cells in Fig. 5E were performed using unpaired two-tailed Student's *t*-test. P values < 0.05 were considered to be statistically significant.

The list of key reagents/resources is available in the key resources table.

3. Results

3.1. Sample acquisition and characterization

To measure changes in chromatin accessibility between freshly isolated and in vitro cultured satellite cells, the latter associated with loss of stem cell properties, we employed ATAC-seq. vastus lateralis muscle biopsies were obtained from human healthy subjects (donor age range 20–50 years old – Table 1) and immediately processed for satellite cell isolation. Human satellite cells can be identified based on the expression of the surface markers CD56 and CD82 (Alexander et al., 2016; Schubert et al., 1989; Uezumi et al., 2016; Marg et al., 2014). As shown in Fig. S1A–B, flow cytometry analysis of the muscle-derived mononuclear fraction identified a clear CD56 + CD82 + population, accounting for approximately 1% of the total. CD56 + CD82 + cells isolated using Fluorescence Activated Cell Sorting (FACS) were characterized by the expression of the satellite cell marker PAX7 (Fig. S1C–D). Once cultured in vitro, these cells acquired a typical myoblast morphology and demonstrated a robust differentiation capability into MYHC + multinucleated myotubes (Fig S1E–F).

3.2. The chromatin accessibility landscape of human activated satellite cells.

Both freshly isolated (human activated satellite cells) and 12-day cultured (myoblasts) were processed for ATAC-seq (Buenrostro et al., 2015). We identified 44,478 loci characterized by differential chromatin accessibility between freshly-isolated and 12-day cultured cells (Fig. 1A and Table S2). Unbiased hierarchical clustering classified these loci into two groups based on higher chromatin accessibility in human activated satellite cells (Group 1 – 11,400 loci) and myoblasts (Group 2 – 33,078 loci), respectively (hereafter referred as up-Fresh and up-Cultured). Loss of chromatin accessibility occurred at the loci encoding known regulators of satellite cell function, such as the transcription factors PAX7, the growth factor VEGFA (Verma et al., 2018), and the receptor NOTCH2 (Fujimaki et al., 2018) (Fig. S2A). In further support of our ability to identify relevant genomic targets underlying human muscle stem cell potential, this epigenetic analysis detected several satellite cell-specific elements in the genomic loci encoding CHRDL2, NFIA, NDRG2 and DUSP1 (Fig. 1B and S2A), genes previously identified as downregulated following in vitro culture of human satellite cells (Charville et al., 2015). As expected, myoblast-specific accessible elements were found at genes encoding known regulators of myogenic differentiation, exemplified by MEF2A, MEF2C and MYOD (Fig. 1B and S2A).

The functional difference among up-Fresh and up-Cultured loci became evident following prediction of transcription factor binding motifs using the MEME-ChIP platform (Bailey et al., 2009). Sequences spanning loci with higher chromatin accessibility in human activated

satellite cells displayed enrichment for motifs recognized by basic leucine zipper proteins (bZIP, e.g. CREB), Nuclear Factor 1 (e.g. NFIA/X), basic helix-loop-helix (bHLH), and NFAT families (Fig. S2B). In contrast, loci in the up-Cultured group displayed enrichment for motifs recognized by regulators of the skeletal myogenic differentiation program such as the Muscle Regulatory Factors (MRFs – MYOD/MYOG/MYF5/MYF6), RUNX, TEAD and MEF2 transcriptional activators (Fig. S2B). In agreement with these observations, gene ontology classification of up-Fresh and up-Cultured elements using GREAT evidenced that genes annotated to Group 1 and 2 loci are associated with Biological Process categories involved in regulation of differentiation and morphogenesis (Fig. S2C). This analysis also revealed that the majority of the loci within both groups are located>5 kilobases away from the nearest TSS (Fig. 1C), suggesting their categorization as transcriptional enhancers. To determine whether the differential ATAC-seq peaks may participate in genomic organization, loci in up-Fresh and up-Cultured groups were compared with available CTCF genomic occupancy data from human primary myoblasts (equivalent to 12-day cultures), as no CTCF ChIP-seq data are available for human satellite cells. CTCF occupies both topologically associated domain (TAD) borders and intra-TAD elements involved in promoter and enhancer insulation (Rowley and Corces, 2018). As shown in Fig. 1D, only a limited fraction of ATAC-seq peaks overlapped with CTCF bound sites, thus suggesting that differential chromatin accessibility occurs at loci with distinct epigenetic features (discussed in murine satellite cell section).

To identify whether differential chromatin accessibility is associated with changes in gene expression, we took advantage of available transcriptomic studies performed in freshly-isolated and cultured human satellite cells (Charville et al., 2015). Analysis of this dataset detected 2,846 differentially expressed transcripts, 527 of them (equivalent to 19%) displaying differential chromatin accessibility at the promoter level (Fig S2D). As expected, decreased and increased chromatin accessibility at the promoter elements were respectively associated with transcripts down- and up-regulated in freshly-isolated and cultured cells (Fig. 1E). Ingenuity pathway analysis (IPA) classified the 527 differentially expressed genes into several functional categories, including “Gene expression”, “Skeletal and muscular system development and function” and “carbohydrate metabolism” (Fig. 1F). Prediction of the networks controlling the differentially expressed genes identified IGF1 (Fig. 1G), p38, STAT, PGE2 and VEGF among the potential upstream regulators (Fig. S2E). Altogether, these data identify a compendium of relevant genomic loci that may underlie regulation of gene expression in activated human satellite cells.

3.3. Annotation of tissue- and stage-specific chromatin accessible human loci

Tissue-specific gene expression is controlled by a complex interplay among three-dimensional genomic organization, chromatin remodeling and transcriptional complexes (Shlyueva et al., 2014). In particular, given their enrichment for lineage-specific transcription factor binding sites, transcriptional enhancers have acquired a central role in our understanding of transcription. Because increased chromatin accessibility (or nuclease sensitivity) is one of the molecular properties exhibited by enhancer elements, we took advantage of our datasets to identify loci that may underlie tissue- and stage-specific transcriptional control. Using available data from the ENCODE project (Moore et al.,

2020), we performed a differential analysis of chromatin accessibility in a total of 19 specimens representing distinct anatomical structures (Fig. 2A). This comparison revealed distinct sets of chromatin accessible loci in human satellite cells, myoblasts and skeletal muscle, respectively (Fig. 2A–B and Table S3). In agreement with their potential role in regulation of the myogenic lineage, functional annotation of the human satellite cell-specific loci (n = 534) evidenced enrichment for biological process categories associated with skeletal muscle development and cell fate specification (Fig. 2C). Tissue-of-origin biological process specificity was also observed upon functional classification of elements belonging to other clusters (Fig. S3A), thus supporting the ability of this method to discover putative tissue- and stage-specific regulatory regions. Inspection of the satellite cell specific dataset identified elements at the genomic loci encoding for CALCR (Fig 2D) and MEGF10 (Fig. S3B). Putative satellite cell specific elements were also observed at the EDN3 and EDNRB loci, both transcriptionally downregulated following human satellite cell in vitro expansion (Fig. 2D and data not shown). Consistent with the differential chromatin accessibility results, tissue specific elements were detected in proximity of the genomic coordinates encoding for ACTA1 and MYOT, two muscle specific genes (Fig. S3B).

3.4. Chromatin accessibility profiling identifies enhancers in murine satellite cells.

Studies investigating the epigenetic mechanisms controlling satellite cell function have been so far restricted to the murine muscle. To take advantage of available genomic datasets, as well as gain further insight into the properties of the regulatory elements controlling satellite cell regenerative capacity, we next used ATAC-seq to profile chromatin accessibility in the murine system. Satellite cells were isolated from the hindlimb muscles of *Pax7-ZsGreen* mice (Bosnakovski et al., 2008), and ATAC-seq was performed on freshly-isolated and in vitro cultured satellite cells (4-day and 10-day), the latter representing myoblasts. Differential analysis of chromatin accessibility detected two main groups of genomic elements characterized by decreased (Group 1) and increased (Group 2) chromatin accessibility during the transition from fresh to cultured (Fig. 3A and Table S2). Similar to their human counterpart, Group 1 included elements annotated to the genomic regions encoding Chrdl2, Nfia and Pax7 (Fig. 3B and S4A). Group 2 loci, instead, were found at Mef2c (Fig. 3B), and other myogenic genes such as Mef2a, Myog (Fig. S4A). Functional annotation assigned Group 1 loci to genes involved in response to signaling stimuli and control of lineage identity, while Group 2 elements were mainly associated with genes regulating skeletal muscle development and differentiation (Fig. S4B). Accordingly, analysis of the sequences underlying these loci identified enrichment for bZIP, NFAT and PAX motifs in Group 1, and bHLH (MRFs), RUNX, MEF2 and TEAD in Group 2 (Fig. S4C). Integration of chromatin accessibility (this study) and transcriptomic data (from (Ryall et al., 2015) identified 1,196 promoters associated with differentially expressed transcripts (Fig. S4D). Pathway analysis classified these genes into multiple functional categories, including “Skeletal and muscular system development and function” and “Tissue morphology” (Fig. S4E).

Having identified the chromatin accessible loci defining activated satellite cells, we next investigated the properties of these elements by taking advantage of available ChIP-seq datasets for various histone marks (Liu et al., 2013; Ryall et al., 2015; Machado et

al., 2017). H3K27Ac defines enhancers and gene promoters, the latter in combination with H3K4me3. H3K27me3, instead, is deposited by the Polycomb repressive complex and is found at transcriptionally repressed and poised elements. H4K16Ac participates in organization of the chromatin three-dimensional structure and is generally involved in gene activation (for a review of these histone marks, please see (Lawrence et al., 2016). Importantly, the datasets used for this analysis were generated by capturing satellite cells undergoing the transition from quiescent to activated (T0-T3) or activated to cultured (F-C), thus allowing to determine the potential role of the chromatin accessible loci observed using ATAC-seq. As shown in Fig. 3C, this analysis categorized Group 1 elements into 4 clusters of loci characterized by different levels of H3K27AC, H3K27me3, H4K16Ac and H3K4me3. Clusters A and B displayed respectively high and medium levels of H3K27Ac, low H3K4me3 and H3K27me3, and were mainly located>5 kb from the closest TSS (Fig. 3D). In particular, Cluster A loci were associated with decreased H3K27Ac during the quiescent to activated transition (Fig. 3D), indicating that these elements may constitute enhancers regulating satellite cell homeostasis. In contrast, Cluster C loci were mainly proximal to TSSs and displayed increasing levels of H4K16Ac and H3K4me4 during the activated to cultured transition (Fig. 3D). These elements likely represent promoters that will be activated in myoblasts. Lastly, Cluster D loci displayed low deposition of these histone marks (Fig. 3C), suggesting that these elements may participate in different processes. Because satellite cell maintenance requires expression of the transcription factor Pax7, Group 1 chromatin accessible loci were compared to the list of Pax7 peaks detected in mouse ES cell-derived myogenic progenitors, a population endowed with in vivo myogenic regeneration potential (Darabi et al., 2011). This analysis revealed 1,644 peaks shared between the two datasets (Fig. 3E), including an element located in proximity of the Chrdl2 locus (Fig. 3B). Pax7 peak distribution across Clusters A to D was comparable, with a slightly lower frequency for Cluster C (Fig. 3E). Collectively, these data show that loci identified by ATAC-seq include potential regulatory elements of murine activated satellite cells, thus providing a framework to begin decoding genomic regulation of this stem cell population.

3.5. Conservation of chromatin accessible elements between human and murine activated satellite cells.

Although to a lesser extent than coding regions, regulatory elements also display conservation across species and, accordingly, comparative genomic studies, such as the one coordinated by the ENCODE consortium, have provided many insights into the mechanisms controlling tissue-specific gene expression (Moore et al., 2020). We reasoned that human-murine conserved loci may allow the identification of relevant processes controlling the activated satellite cells to cultured myoblasts transition. To address this question, the genomic coordinates representing the differentially accessible loci identified in human cells (Fig. 1) were used to identify synthenic elements in the mouse genome, which yielded 8,883 and 20,839 loci in the up-Fresh and up-Cultured groups, respectively (Fig. 4A). Comparison of these two lists with their murine counterparts (from Fig. 3A) generated 406 and 876 common elements in up-Fresh and up-Cultured groups, respectively (Fig. 4A and Table S4). The majority of these loci was annotated>5 kb from the closest TSS (Fig. 4B and data not shown) and included elements located in proximity of Heyl (Fig. 4C), Chrdl2 and

Mef2c (Fig. 3B). In agreement with the analyses performed on each individual dataset, conserved mouse-human up-Fresh and up-Cultured loci displayed enrichment for motifs recognized by transcription factors participating in satellite cell homeostasis (up-Fresh) and muscle differentiation (up-Cultured - Fig. 4D), such as PAX and MRFs, respectively. In general, expression of these transcription factors correlated with the predicted motif enrichment (Fig. S5A–B). Lastly, footprint analysis for the above mentioned transcription factors evidenced that the overall percentage of potential footprints does not dramatically differ when comparing orthologous murine and human loci for the same time point (Fig. S5C).

3.6. PPARGC1A and other metabolic regulator genes are predicted conserved Pax7 targets in activated satellite cells.

Next, conserved up-Fresh and up-Cultured loci were functionally annotated to determine biological processes associated with these elements. While conserved up-Cultured loci were mainly found near genes involved in striated muscle development, up-Fresh elements were associated with genes controlling biosynthetic and metabolic processes (Fig. 5A). The latter included PPARGC1A. The involvement of this gene is in line with the notion that satellite cell activation involves a coordinated regulation of various metabolic genes (Ryall et al., 2015) and Fig. S6A). Interestingly, conserved human-murine loci characterized by loss of chromatin accessibility during the activated to cultured transition were also found at the KLF15, PPARG, PPARGC1B and PDK4 genomic regions, including promoters (Fig. 5B and data not shown). PDK4, in particular, is one of the kinases regulating the pyruvate dehydrogenase complex, which links the glycolytic pathway to the oxidative phosphorylation machinery (Linn et al., 1969). Because some of these elements directly overlapped, or were in proximity, to potential Pax7 binding sites (Fig. 5B), we speculated that these genes may represent targets of this transcription factor. In support of this hypothesis, most of these genes were differentially expressed during the transition from quiescent to activated or activated to cultured in both murine (Fig. 5C and S6B) and human (Fig S6C) satellite cells. To validate whether Pax7 directly controls these genes, freshly sorted murine satellite cells were transduced with a lentivirus encoding Pax7 or GFP (ctrl), expanded in vitro and then collected for RNA analysis. While Klf15 levels were not changed, both Ppargc1a and Pparg levels were downregulated following Pax7 over-expression (Fig. 5D), suggesting that this transcription factor controls the activation status of elements regulating expression of key metabolic genes. Altogether, these observations provide strong evidence that human and murine satellite cells and myoblasts share a subset of regulatory networks, involving conserved genomic elements and molecular effectors, and predict new Pax7 targets underlying the metabolic control of satellite cells.

4. Discussion

In this study we describe the chromatin accessibility profiles of activated human satellite cells and myoblasts. There is a critical need to enhance our understanding of human satellite cell biology, as these cells represent a potential therapeutic population for treating muscle disorders. To date, studies aimed at decoding the epigenetic mechanisms controlling satellite cell properties have been restricted to the murine muscle. Through analysis of chromatin

accessibility, we identified a compendium of potential regulatory elements associated with gene regulation in satellite cells. By comparing the chromatin accessibility profile of human satellite cells with available ATAC-seq datasets from the ENCODE consortium, our analyses defined a subset of human activated satellite cell elements located near genes downregulated following in vitro culture. Following investigation of the chromatin accessibility changes occurring during murine satellite cell activation and the integration of these data with histone profiling studies, we identified conserved elements characterizing human and murine activated satellite cells and myoblasts. Altogether, our approach defines a list of putative regulatory elements controlling human activated satellite cells, thus providing a basic mechanistic understanding, as well as a platform for the future discovery, of novel mechanisms controlling muscle regenerative potential.

In terms of regenerative potential, human satellite cells are the ideal cell population for cell-based interventions to treat patients with muscle disorders (Biressi et al., 2020). However, a major caveat for the clinical application of these cells remains the lack of proper culture conditions able to ensure in vitro expansion without loss of stem cell properties. Over the past few years, various studies have contributed to the characterization of human satellite cells, including identification of surface markers, analysis of regenerative potential, transcriptomic and cell heterogeneity studies (Alexander et al., 2016; Uezumi et al., 2016; Marg et al., 2014; Charville et al., 2015; Garcia et al., 2018; Barruet et al., 2020; Xu et al., 2015; De Micheli et al., 2020; Feige et al., 2021). Nonetheless, our knowledge of the epigenetic mechanisms controlling sternness in human satellite cells remains limited. We believe that deciphering the regulatory landscape of satellite cells will be critical for developing new strategies aimed at promoting muscle regeneration. To begin addressing this question, we determined the first chromatin accessibility profile of human satellite cells freshly isolated from an adult muscle. We used these epigenetic data to identify differential chromatin accessible loci between satellite cells and myoblasts and, through integration with available transcriptomic data, we began defining the transcriptional networks active in human satellite cells.

Analysis of upstream regulators controlling human activated satellite cells identified a subset of effectors previously reported to control murine satellite cell activation and homeostasis, including p38, STAT3, PGE2 and VEGFA. The p38 kinase is quickly activated upon satellite cell activation and controls loss of quiescence (Bernet et al., 2014; Cosgrove et al., 2014). The Jak/Stat pathway represses symmetric satellite cells division, and inhibition of Stat3 enhances symmetric cell division in vitro and engraftment in vivo (Price et al., 2014; Tierney et al., 2014). PGE2 signaling controls satellite cell expansion during muscle regeneration by triggering CREB activation, which in turn induces the pro-proliferative transcription factor Nurr1 (Ho et al., 2017). VEGF, secreted by the satellite cells, plays a critical role in maintaining quiescence through crosstalk with the vascular niche (Verma et al., 2018). Because genes associated with these pathways have been identified based on their differential chromatin accessibility and expression, we speculate that additional molecules arising from our analysis may be involved in satellite cell regulation. This list includes the endothelin pathway. Accordingly, EDN3 has been identified in independent transcriptomic studies aimed at determining murine satellite cell specific transcripts (Fukada et al., 2007; Pannerec et al., 2013), and its mRNA is downregulated as satellite cells exit

quiescence (Machado et al., 2017; van Velthoven et al., 2017). Our analyses revealed a satellite cell specific element at the EDN3 locus, and both EDN3 and its receptor EDNRB are downregulated following human satellite cell in vitro culture. EDN3 mutations are known in Waardenburg syndrome type IV patients and, in general, underlie defects in enteric nervous system and melanocyte development (reviewed in (Bondurand et al., 2018). Nonetheless, the endothelin system has broader physiological and pathological functions. For example, EDN3 and EDNRB have been reported to control cell proliferation and self-renewal in glioblastoma through an autocrine signaling mechanism (Liu et al., 2011). Since the majority of Edn3 knockout mice die within one month after birth, likely due to altered colon development (Baynash et al., 1994), there are no indications whether this pathway is required for satellite cells homeostasis.

Other potential candidates predicted by these studies include factors controlling metabolic gene expression. Previous analyses found that murine satellite cells are in a quiescent metabolic state and, following activation, they switch from fatty acid oxidation to glycolysis. This transition is associated with an increase in NAD + which, in turn, represses the histone deacetylase Sirt1 and leads to accumulation of the H4K16Ac mark at myogenic loci (Ryall et al., 2015). The metabolic state of these cells changes also as a function of age, with satellite cells isolated from old mice relying more on glycolysis than oxidative phosphorylation (Pala et al., 2018). Our studies found that PPARGC1A, PPARG and KLF15 displayed differential chromatin accessibility and gene expression in the transition from activated satellite cells to myoblasts. Ppargc1a and Klf15 have been shown to directly upregulate the expression of multiple metabolic genes in skeletal muscle, including Pdk4 (Prosdocimo et al., 2014; Wende et al., 2005), and transgenic mice expressing either Ppargc1a or Klf15 under a muscle-specific promoter display improved exercise endurance capacity (Haldar et al., 2012; Lin et al., 2002). In agreement with the transcriptional changes reported in previous studies (Ryall et al., 2015; Yucel et al., 2019), we also observed that satellite cell activation is accompanied by differential chromatin accessibility at the genomic loci encoding metabolic enzymes, such as PDK4 and others. Pdk4 has been recently implicated in the regulation of global histone acetylation levels in myogenic cells undergoing differentiation, and lack of both Pdk2 and 4 impairs satellite cell regenerative capacity due to a diminished myogenic differentiation potential (Yucel et al., 2019). Notably, our analyses predict Pax7 occupancy at a subset of loci with differentially accessible chromatin annotated to these metabolic genes, thus suggesting the direct involvement of this transcription factor in the expression of genes regulating the metabolic switch observed during satellite cell activation.

In myogenic cells, Pax7 binding to its cognate sites is associated with increased chromatin accessibility and deposition of histone marks promoting gene activation (Lilja et al., 2017). Through chromatin looping, these elements constitute regulatory hubs controlling myogenic gene expression. Following loss of Pax7 and consequent differentiation into myotubes, a fraction of the Pax7-regulated elements maintains an active epigenetic signature and participates in gene activation (Lilja et al., 2017; Zhang et al., 2020). This is exemplified by the Pax7-bound regulatory element located within the myosin heavy chain locus which, upon Pax7 loss, contacts and activates the promoters of the nearby myosin genes (Zhang et al., 2020). Although genome occupancy data for Pax7 in adult satellite cells are still

not available, these studies in ES cell-derived myogenic progenitors support the notion that Pax7 (as well as its homolog Pax3) controls regulatory networks underlying activation and repression of gene expression by coordinating chromatin remodeling and looping (Zhang et al., 2020; Magli et al., 2019). Since transcriptomic studies reported that several genes are quickly expressed upon satellite cell activation (Machado et al., 2017; van Velthoven et al., 2017), and our analysis shows that Ppargc1a and Pparg are down-regulated following Pax7 overexpression, we speculate that these genes are controlled by Pax7 in quiescent satellite cells, which may be required for finely tuning the activation of metabolic pathways as cells exit quiescence. Future studies, such as satellite cell-specific deletion of these candidate, will enable the decoding of these molecular events.

An important corollary of our analysis is the identification of human satellite cell-specific chromatin accessible elements. Control of cell- and tissue-specific gene expression relies on a multitude of regulatory elements which, in many cases, are located several kilobases upstream or downstream the TSS. While a systematic effort aimed at cataloging all of the regulatory genome is greatly contributing to our understanding of gene expression in several tissues (Moore et al., 2020), there are still few available datasets for rare populations such as human satellite cells. By comparing the chromatin accessibility profile of human satellite cells with datasets from the ENCODE consortium, our analyses identified a subset of elements that may participate in the control of gene expression in satellite cells. This list includes elements located at the genomic regions encoding for genes controlling satellite cell quiescence, as in the case of CALCR and MEGF10. CALCR-mediated signaling is necessary for maintaining satellite dormancy, which involves its interaction with Collagen V located in the muscle niche (Baghdadi et al., 2018; Yamaguchi et al., 2015). MEGF10 is a NOTCH-interacting transmembrane protein essential for preventing precocious satellite cell differentiation (Holterman et al., 2007; Saha et al., 2017). Specific elements were identified also for other samples, as in the case of genes expressed in terminally differentiated skeletal muscle cells, such as *ACTA1*. Collectively, our analysis identifies potential satellite cell-specific regulatory elements that, if integrated in transgenic constructs, could be useful for directing gene expression in this cell population.

5. Conclusions

Our findings provide new insights on the molecular regulation of human satellite cells and represent a starting point for future studies aimed at investigating the human satellite cell epigenome. As more data regarding this muscle stem cell population become available, such as the recent identification of specific subpopulations of human satellite cells using single cell transcriptomics (Barruet et al., 2020; De Micheli et al., 2020), we hope ultimately to overcome the barriers preventing the effective clinical use of human satellite cells for the treatment of muscle regenerative disorders.

Supplementary Material

Refer to Web version on PubMed Central for supplementary material.

Acknowledgements

The authors would like to thank Dr. June Baik for critical reading of the manuscript.

Funding

This work has been supported by a research grant from the Greg Marzolf Junior Foundation (A.M.), and a Grant-in-aid from the University of Minnesota Office of Vice President Research (A.M.). Funding for the sample acquisition was supported by the National Institutes of Health (L.S.C. 1R01DK098203). In addition, research reported in this publication was supported by the National Center for Advancing Translational Sciences of the NIH - Award Number UL1TR000114. R.C.R.P. was supported by NIH R01 AR071439 and R56 AR055299. M.K was supported by NIH R01 AR055685. The content is solely the responsibility of the authors and does not necessarily represent the official views of the National Institutes of Health.

Availability of data and materials

Sequencing data generated in this work are available from the GEO database under the accession number (GSE165414). CTCF genomic occupancy in human myoblasts (ENCFF586KHT and ENCFF741PXH) and ATAC-seq data for different human tissues were downloaded from the ENCODE portal (www.encodeproject.org). Other data used in this manuscript were previously deposited under the accession numbers: GSE103163 (H3K27Ac and H3K27me3 in *in situ* fixed and 3-hour post-isolation fixed murine satellite cells); GSE47362 (H3K4me3 and H3K27me3 in freshly-isolated and cultured satellite cells); GSE64379 (H4K16Ac in freshly-isolated and cultured satellite cells); GSE147057 (Pax7 genomic occupancy in ES cell-derived myogenic progenitors): GSE89977 (ATAC-seq freshy-isolated murine satellite cells).

Abbreviations:

ATAC-seq	Assay for Transposase Accessible Chromatin followed by sequencing
bHLH	basic helix-loop-helix
bZIP	basic leucine zipper
CALCR	Calcitonin Receptor
CHRDL2	Chordin like 2
ChIP-seq	Chromatin immunoprecipitation followed by sequencing
DUSP1	Dual-specificity phosphatase 1
EDN3	Endothelin-3
EDNRB	Endothelin Receptor B
ES cells	Embryonic Stem cells
H3K4me3	Histone H3 trimethylated on lysine 4
H3K27Ac	Histone H3 acetylated on lysine 27

H3K27me3	Histone H3 trimethylated on lysine 27
H4K16Ac	Histone H4 acetylated on lysine 16
IGF1	Insulin Like Growth Factor 1
KLF15	Kruppel like factor 15
MEF2	Myocyte enhancer factor 2
MEGF10	Multiple epidermal growth factor-like domains protein 10
MRFs	Muscle Regulatory Factors
MYHC	Myosin heavy chain
NDRG2	N-myc downstream regulated gene 2
NFAT	Nuclear factor of activated T cells
NFIA	Nuclear factor 1A
PAX7	Paired box 7
PDK4	Pyruvate dehydrogenase kinase 4
PGE2	Prostaglandin E2
PHDA1	Pyruvate Dehydrogenase subunit A1
PPARG	Peroxisome proliferator-activated receptor gamma
PPARGC1A	Peroxisome proliferator-activated receptor gamma coactivator 1-alpha – usually referred as PGC1α
TSS	Transcription start site
VEGF	Vascular endothelial growth factor

References

Feige P, Brun CE, Ritso M, Rudnicki MA, 2018. Orienting Muscle Stem Cells for Regeneration in Homeostasis. Aging, and Disease, Cell Stem Cell 23, 653–664. [PubMed: 30388423]

Reimann J, Brimah K, Schroder R, Wernig A, Beauchamp JR, Partridge TA, 2004. Pax7 distribution in human skeletal muscle biopsies and myogenic tissue cultures. Cell Tissue Res. 315, 233–242. [PubMed: 14648195]

Seale P, Sabourin LA, Girgis-Gabardo A, Mansouri A, Gruss P, Rudnicki MA, 2000. Pax7 is required for the specification of myogenic satellite cells. Cell 102, 777–786. [PubMed: 11030621]

Montarras D, Morgan J, Collins C, Relaix F, Zaffran S, Cumano A, Partridge T, Buckingham M, 2005. Direct isolation of satellite cells for skeletal muscle regeneration. Science 309, 2064–2067. [PubMed: 16141372]

Sacco A, Doyonnas R, Kraft P, Vitorovic S, Blau HM, 2008. Self-renewal and expansion of single transplanted muscle stem cells. Nature 456, 502–506. [PubMed: 18806774]

Liu L, Cheung T, Charville G, Hurgo B, Leavitt T, Shih J, Brunet A, Rando T, 2013. Chromatin modifications as determinants of muscle stem cell quiescence and chronological aging. Cell Rep. 4 (1), 189–204. [PubMed: 23810552]

Shcherbina A, Larouche J, Fraczek P, Yang BA, Brown LA, Markworth JF, Chung CH, Khaliq M, de Silva K, Choi JJ, Fallahi-Sichani M, Chandrasekaran S, Jang YC, Brooks SV, Aguilar CA, 2020. Dissecting murine muscle stem cell aging through regeneration using integrative genomic analysis. Cell Rep. 32 (4), 107964. 10.1016/j.celrep.2020.107964. [PubMed: 32726628]

Ryall J, Dell'Orso S, Derfoul A, Juan A, Zare H, Feng X, Clermont D, Koulnis M, Gutierrez-Cruz G, Fulco M, Sartorelli V, 2015. The NAD(+)-dependent SIRT1 deacetylase translates a metabolic switch into regulatory epigenetics in skeletal muscle stem cells. Cell Stem Cell 16 (2), 171–183. [PubMed: 25600643]

Machado L, Esteves de Lima J, Fabre O, Proux C, Legendre R, Szegedi A, Varet H, Ingerslev LR, Barrès R, Relaix F, Mourikis P, 2017. In situ fixation redefines quiescence and early activation of skeletal muscle stem cells. Cell Rep. 21 (7), 1982–1993. [PubMed: 29141227]

van Velthoven CTJ, de Morree A, Egner IM, Brett JO, Rando TA, 2017. Transcriptional profiling of quiescent muscle stem cells in vivo. Cell Rep. 21, 1994–2004. [PubMed: 29141228]

Buenrostro JD, Giresi PG, Zaba LC, Chang HY, Greenleaf WJ, 2013. Transposition of native chromatin for fast and sensitive epigenomic profiling of open chromatin, DNA-binding proteins and nucleosome position. Nat. Methods 10, 1213–1218. [PubMed: 24097267]

Shlyueva D, Stampfel G, Stark A, 2014. Transcriptional enhancers: from properties to genome-wide predictions. Nat. Rev. Genet 15, 272–286. [PubMed: 24614317]

Buenrostro JD, Wu B, Chang HY, Greenleaf WJ, ATAC-seq: A Method for Assaying Chromatin Accessibility Genome-Wide, Curr. Protoc. Mol. Biol, 109 (2015) 21 29 21–29.

Bosnakovski D, Xu Z, Li W, Thet S, Cleaver O, Perlingeiro RC, Kyba M, 2008. Prospective isolation of skeletal muscle stem cells with a Pax7 reporter. Stem Cells 26, 3194–3204. [PubMed: 18802040]

Li Z, Schulz MH, Look T, Begemann M, Zenke M, Costa IG, 2019. Identification of transcription factor binding sites using ATAC-seq. Genome Biol. 20, 45. [PubMed: 30808370]

Alexander MS, Rozkalne A, Colletta A, Spinazzola JM, Johnson S, Rahimov F, Meng H, Lawlor MW, Estrella E, Kunkel LM, Gussoni E, 2016. CD82 Is a marker for prospective isolation of human muscle satellite cells and is linked to muscular dystrophies. Cell Stem Cell 19 (6), 800–807. [PubMed: 27641304]

Schubert W, Zimmermann K, Cramer M, Starzinski-Powitz A, 1989. Lymphocyte antigen Leu-19 as a molecular marker of regeneration in human skeletal muscle. Proc. Natl. Acad. Sci. U. S. A 86 (1), 307–311. [PubMed: 2463624]

Uezumi A, Nakatani M, Ikemoto-Uezumi M, Yamamoto N, Morita M, Yamaguchi A, Yamada H, Kasai T, Masuda S, Narita A, Miyagoe-Suzuki Y, Takeda S, Fukada S-I, Nishino I, Tsuchida K, 2016. Cell-surface protein profiling identifies distinctive markers of progenitor cells in human skeletal muscle. Stem Cell Rep. 7 (2), 263–278.

Marg A, Escobar H, Gloy S, Kufeld M, Zacher J, Spuler A, Birchmeier C, Izsvák Z, Spuler S, 2014. Human satellite cells have regenerative capacity and are genetically manipulable. J. Clin. Invest 124 (10), 4257–4265. [PubMed: 25157816]

Verma M, Asakura Y, Murakonda BSR, Pengo T, Latroche C, Chazaud B, McLoon LK, Asakura A, 2018. Muscle satellite cell cross-talk with a vascular niche maintains quiescence via VEGF and notch signaling. Cell Stem Cell 23 (4), 530–543. e9. [PubMed: 30290177]

Fujimaki S, Seko D, Kitajima Y, Yoshioka K, Tsuchiya Y, Masuda S, Ono Y, 2018. Notch1 and Notch2 coordinately regulate stem cell function in the quiescent and activated states of muscle satellite cells. Stem Cells 36 (2), 278–285. [PubMed: 29139178]

Charville GW, Cheung TH, Yoo B, Santos PJ, Lee GK, Shrager JB, Rando TA, 2015. Ex vivo expansion and in vivo self-renewal of human muscle stem cells. Stem Cell Rep. 5, 621–632.

Bailey TL, Boden M, Buske FA, Frith M, Grant CE, Clementi L, Ren J, Li WW, Noble WS, 2009. MEME SUITE: tools for motif discovery and searching. Nucleic Acids Res. 37 (Web Server), W202–W208. [PubMed: 19458158]

Rowley MJ, Corces VG, 2018. Organizational principles of 3D genome architecture. Nat. Rev. Genet 19 (12), 789–800. [PubMed: 30367165]

Moore JE, Purcaro MJ, Pratt HE, Epstein CB, Shoresh N, Adrian J, Kawli T, Davis CA, Dobin A, Kaul R, Halow J, Van Nostrand EL, Freese P, Gorkin DU, Shen Y, He Y, Mackiewicz M, Pauli-Behn

F, Williams BA, Mortazavi A, Keller CA, Zhang X-O, Elhajjajy SI, Huey J, Dickel DE, Snetkova V, Wei X, Wang X, Rivera-Mulia JC, Rozowsky J, Zhang J, Chhetri SB, Zhang J, Victorsen A, White KP, Visel A, Yeo GW, Burge CB, Lécuyer E, Gilbert DM, Dekker J, Rinn J, Mendenhall EM, Ecker JR, Kellis M, Klein RJ, Noble WS, Kundaje A, Guigó R, Farnham PJ, Cherry JM, Myers RM, Ren B, Graveley BR, Gerstein MB, Pennacchio LA, Snyder MP, Bernstein BE, Wold B, Hardison RC, Gingeras TR, Stamatoyannopoulos JA, Weng Z, 2020. Expanded encyclopaedias of DNA elements in the human and mouse genomes. Nature 583 (7818), 699–710. [PubMed: 32728249]

Lawrence M, Daujat S, Schneider R, 2016. Lateral thinking: how histone modifications regulate gene expression. Trends Genet. 32, 42–56. [PubMed: 26704082]

Darabi R, Santos FN, Filareto A, Pan W, Koene R, Rudnicki MA, Kyba M, Perlingeiro RC, 2011. Assessment of the myogenic stem cell compartment following transplantation of Pax3/Pax7-induced embryonic stem cell-derived progenitors. Stem Cells 29, 777–790. [PubMed: 21374762]

Linn TC, Pettit FH, Reed LJ, 1969. Alpha-keto acid dehydrogenase complexes. X. Regulation of the activity of the pyruvate dehydrogenase complex from beef kidney mitochondria by phosphorylation and dephosphorylation. Proc. Natl. Acad. Sci. U. S. A 62, 234–241. [PubMed: 4306045]

Biressi S, Filareto A, Rando TA, 2020. Stem cell therapy for muscular dystrophies. J. Clin. Invest 130, 5652–5664. [PubMed: 32946430]

Garcia SM, Tamaki S, Lee S, Wong A, Jose A, Dreux J, Kouklis G, Sbitany H, Seth R, Knott PD, Heaton C, Ryan WR, Kim EA, Hansen SL, Hoffman WY, Pomerantz JH, 2018. High-yield purification, preservation, and serial transplantation of human satellite cells. Stem Cell Reports 10, 1160–1174. [PubMed: 29478895]

Barruet E, Garcia SM, Striedinger K, Wu J, Lee S, Byrnes L, Wong A, Xuefeng S, Tamaki S, Brack AS, Pomerantz JH, 2020. Functionally heterogeneous human satellite cells identified by single cell RNA sequencing. Elife 9.

Xu X, Wilschut K, Kouklis G, Tian H, Hesse R, Garland C, Sbitany H, Hansen S, Seth R, Knott PD, Hoffman W, Pomerantz J, 2015. Human satellite cell transplantation and regeneration from diverse skeletal muscles. Stem Cell Rep. 5 (3), 419–434.

De Micheli AJ, Spector JA, Elemento O, Cosgrove BD, A reference single-cell transcriptomic atlas of human skeletal muscle tissue reveals bifurcated muscle stem cell populations, bioRxiv, (2020) 2020.2001.2021.914713.

Feige P, Tsai EC, Rudnicki MA, 2021. Analysis of human satellite cell dynamics on cultured adult skeletal muscle myofibers. Skelet Muscle 11, 1. [PubMed: 33397479]

Bernet JD, Doles JD, Hall JK, Kelly Tanaka K, Carter TA, Olwin BB, 2014. p38 MAPK signaling underlies a cell-autonomous loss of stem cell self-renewal in skeletal muscle of aged mice. Nat. Med 20 (3), 265–271. [PubMed: 24531379]

Cosgrove BD, Gilbert PM, Porpiglia E, Mourkioti F, Lee SP, Corbel SY, Llewellyn ME, Delp SL, Blau HM, 2014. Rejuvenation of the muscle stem cell population restores strength to injured aged muscles. Nat. Med 20, 255–264. [PubMed: 24531378]

Price FD, von Maltzahn J, Bentzinger CF, Dumont NA, Yin H, Chang NC, Wilson DH, Frenette J, Rudnicki MA, 2014. Inhibition of JAK-STAT signaling stimulates adult satellite cell function. Nat. Med 20, 1174–1181. [PubMed: 25194569]

Tierney MT, Aydogdu T, Sala D, Malecova B, Gatto S, Puri PL, Latella L, Sacco A, 2014. STAT3 signaling controls satellite cell expansion and skeletal muscle repair. Nat. Med 20, 1182–1186. [PubMed: 25194572]

Ho ATV, Palla AR, Blake MR, Yucel ND, Wang YX, Magnusson KEG, Holbrook CA, Kraft PE, Delp SL, Blau HM, 2017. Prostaglandin E2 is essential for efficacious skeletal muscle stem-cell function, augmenting regeneration and strength. Proc. Natl. Acad. Sci. U. S. A 114, 6675–6684. [PubMed: 28607093]

Fukada S, Uezumi A, Ikemoto M, Masuda S, Segawa M, Tanimura N, Yamamoto H, Miyagoe-Suzuki Y, Takeda S, 2007. Molecular signature of quiescent satellite cells in adult skeletal muscle. Stem Cells 25, 2448–2459. [PubMed: 17600112]

Pannerec A, Formicola L, Besson V, Marazzi G, Sassoon DA, 2013. Defining skeletal muscle resident progenitors and their cell fate potentials. Development 140, 2879–2891. [PubMed: 23739133]

Bondurand N, Dufour S, Pingault V, 2018. News from the endothelin-3/EDNRB signaling pathway: Role during enteric nervous system development and involvement in neural crest-associated disorders. Dev. Biol 444 (Suppl 1), S156–S169. [PubMed: 30171849]

Liu Y, Ye F, Yamada K, Tso JL, Zhang Y, Nguyen DH, Dong Q, Soto H, Choe J, Dembo A, Wheeler H, Eskin A, Schmid I, Yong WH, Mischel PS, Cloughesy TF, Kornblum HI, Nelson SF, Liau LM, Tso C-L, 2011. Autocrine endothelin-3/endothelin receptor B signaling maintains cellular and molecular properties of glioblastoma stem cells. Mol. Cancer Res 9 (12), 1668–1685. [PubMed: 22013079]

Baynash AG, Hosoda K, Giaid A, Richardson JA, Emoto N, Hammer RE, Yanagisawa M, 1994. Interaction of endothelin-3 with endothelin-B receptor is essential for development of epidermal melanocytes and enteric neurons. Cell 79 (7), 1277–1285. [PubMed: 8001160]

Pala F, Di Girolamo D, Mella S, Yennek S, Chatre L, Ricchetti M, Tajbakhsh S, 2018. Distinct metabolic states govern skeletal muscle stem cell fates during prenatal and postnatal myogenesis. J. Cell Sci 131.

Prosdocimo DA, Anand P, Liao X, Zhu H, Shelkay S, Artero-Calderon P, Zhang L, Kirsh J, Moore D, Rosea MG, Vazquez E, Kerner J, Akat KM, Williams Z, Zhao J, Fujioka H, Tuschl T, Bai X, Schulze PC, Hoppel CL, Jain MK, Haldar SM, 2014. Kruppel-like factor 15 is a critical regulator of cardiac lipid metabolism. J. Biol. Chem 289, 5914–5924. [PubMed: 24407292]

Wende AR, Huss JM, Schaeffer PJ, Giguere V, Kelly DP, 2005. PGC-1alpha coactivates PDK4 gene expression via the orphan nuclear receptor ERRalpha: a mechanism for transcriptional control of muscle glucose metabolism. Mol. Cell. Biol 25, 10684–10694. [PubMed: 16314495]

Haldar SM, Jeyaraj D, Anand P, Zhu H, Lu Y, Prosdocimo DA, Eapen B, Kawanami D, Okutsu M, Brotto L, Fujioka H, Kerner J, Rosea MG, McGuinness OP, Snow RJ, Russell AP, Gerber AN, Bai X, Yan Z, Nosek TM, Brotto M, Hoppel CL, Jain MK, 2012. Kruppel-like factor 15 regulates skeletal muscle lipid flux and exercise adaptation. Proc. Natl. Acad. Sci. U. S. A 109, 6739–6744. [PubMed: 22493257]

Lin J, Wu H, Tarr PT, Zhang CY, Wu Z, Boss O, Michael LF, Puigserver P, Isotani E, Olson EN, Lowell BB, Bassel-Duby R, Spiegelman BM, 2002. Transcriptional co-activator PGC-1 alpha drives the formation of slow-twitch muscle fibres. Nature 418, 797–801. [PubMed: 12181572]

Yucel N, Wang YX, Mai T, Porpiglia E, Lund PJ, Markov G, Garcia BA, Bendall SC, Angelo M, Blau HM, 2019. Glucose metabolism drives histone acetylation landscape transitions that dictate muscle stem cell function. Cell Rep. 27, 3939–3955 e3936. [PubMed: 31242425]

Lilja KC, Zhang N, Magli A, Gunduz V, Bowman CJ, Arpke RW, Darabi R, Kyba M, Perlingeiro R, Dynlacht BD, Asakura A, 2017. Pax7 remodels the chromatin landscape in skeletal muscle stem cells. PLoS ONE 12 (4), e0176190. [PubMed: 28441415]

Zhang N, Mendieta-Esteban J, Magli A, Lilja KC, Perlingeiro RCR, Marti-Renom MA, Tsirigos A, Dynlacht BD, 2020. Muscle progenitor specification and myogenic differentiation are associated with changes in chromatin topology. Nat. Commun 11, 6222. [PubMed: 33277476]

Magli A, Baik J, Pota P, Cordero CO, Kwak IY, Garry DJ, Love PE, Dynlacht BD, Perlingeiro RCR, 2019. Pax3 cooperates with Ldb1 to direct local chromosome architecture during myogenic lineage specification. Nat. Commun 10, 2316. [PubMed: 31127120]

Baghdadi MB, Castel D, Machado L, Fukada SI, Birk DE, Relaix F, Tajbakhsh S, Mourikis P, 2018. Reciprocal signalling by Notch-Collagen V-CALCR retains muscle stem cells in their niche. Nature 557, 714–718. [PubMed: 29795344]

Yamaguchi M, Watanabe Y, Ohtani T, Uezumi A, Mikami N, Nakamura M, Sato T, Ikawa M, Hoshino M, Tsuchida K, Miyagoe-Suzuki Y, Tsujikawa K, Takeda S, Yamamoto H, Fukada S, 2015. Calcitonin receptor signaling inhibits muscle stem cells from escaping the quiescent state and the niche. Cell Rep. 13, 302–314. [PubMed: 26440893]

Holterman CE, Le Grand F, Kuang S, Seale P, Rudnicki MA, 2007. Megf10 regulates the progression of the satellite cell myogenic program. J. Cell Biol 179, 911–922. [PubMed: 18056409]

Saha M, Mitsuhashi S, Jones MD, Manko K, Reddy HM, Bruels CC, Cho KA, Pacak CA, Draper I, Kang PB, 2017. Consequences of MEGF10 deficiency on myoblast function and Notch1 interactions. Hum. Mol. Genet 26, 2984–3000. [PubMed: 28498977]

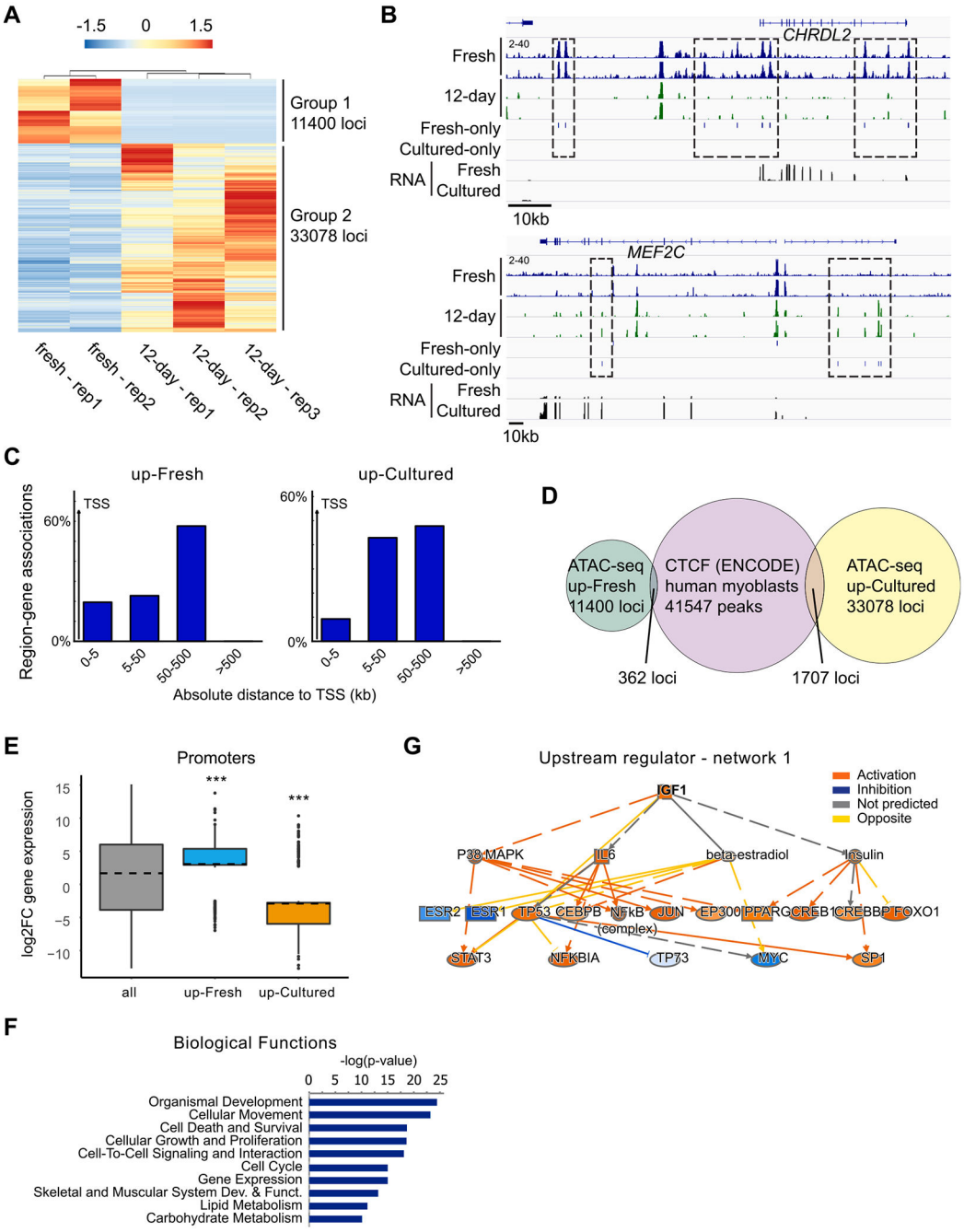

Fig. 1.

The chromatin accessibility landscape of human activated satellite cells and myoblasts. **A**) Heatmap displaying the differential accessible loci between freshly-isolated human satellite cells (2 independent subsets) and myoblasts (3 independent subsets). Group 1 and 2 indicate loci characterized by loss and gain of accessibility during the transition from freshly-isolated (activated) satellite cells and cultured myoblasts, respectively. **B**) IGV track displaying chromatin accessibility and RNA expression at the *CHRDL2* and *MEF2C* loci in human freshly-isolated satellite cells (fresh) and myoblasts (cultured). Dashed black

squares indicate differential accessible loci (reported in the Fresh-only and Cultured-only tracks). **C**) Genomic annotation of Fresh- and Cultured-only loci. Distance from TSS is expressed in kilobases (kb). **D**) Venn diagram displaying the comparison among up-Fresh and up-Cultured loci with CTCF ChIP-seq ENCODE data for human myoblasts. **E**) Box plot representing the gene expression changes (log2FC fresh/cultured) in promoters characterized by increased chromatin accessibility in freshly-isolated human satellite cells (up-fresh) and myoblasts (up-cultured). Statistical differences are relative to group representing all differentially expressed genes (all). ***$p < 0.001$. **F**) Selected top biological functions identified following IPA core analysis of the differential expressed genes characterized by changes in promoter chromatin accessibility (from Fig. S2D) during the activated satellite cells to myoblasts transition. **G**) Example of upstream regulators predicted by the core analysis. Other predicted regulators are reported in Fig. S2E.

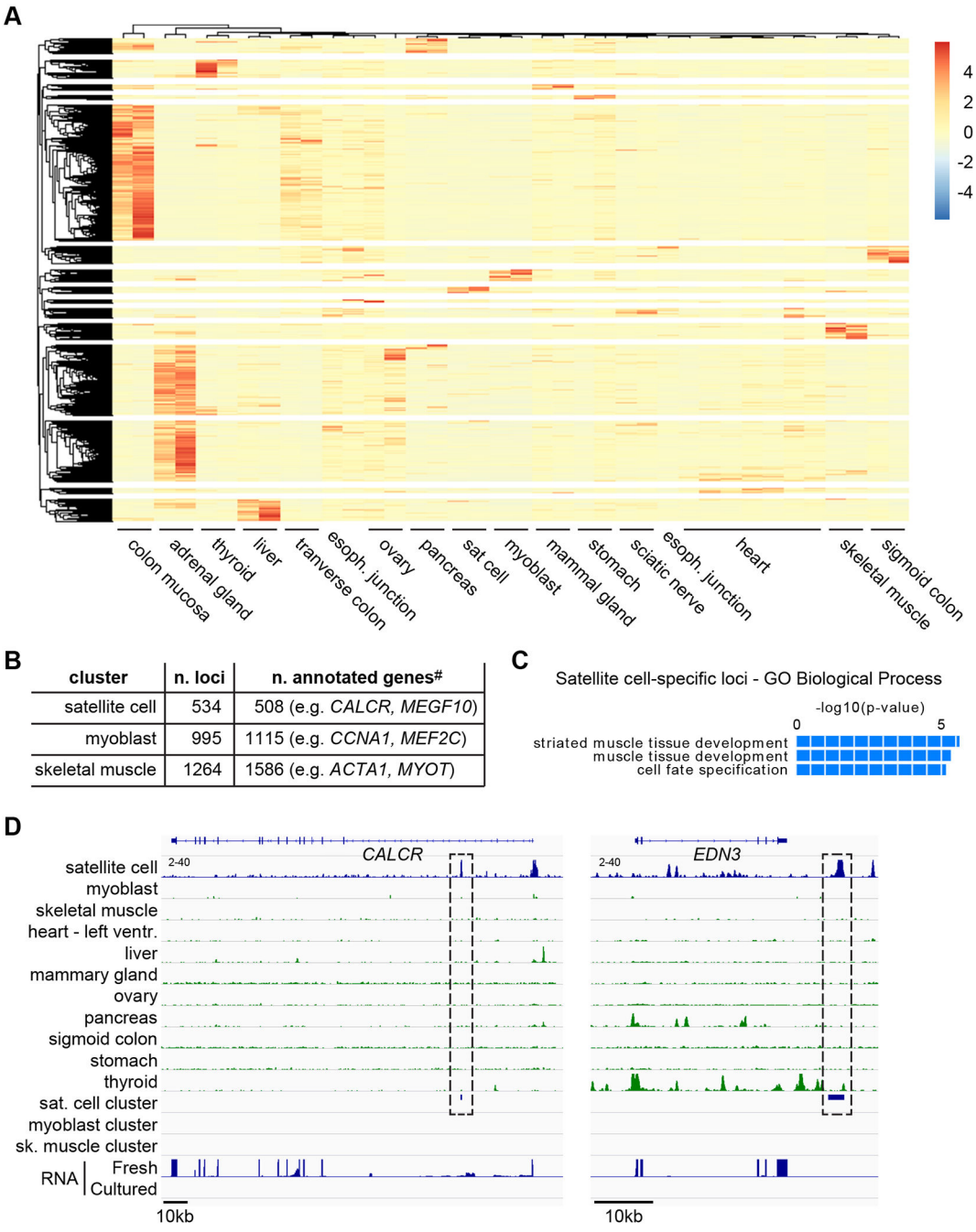

Fig. 2.

Annotation of tissue- and stage-specific chromatin accessible loci. **A**) Heatmap displaying the differential accessible loci between freshly-isolated human satellite cells and various tissues (from ENCODE data). Each sample consisted of 2 independent replicates. **B)** Schematic table reporting number of loci identified in satellite cell-, myoblast- and skeletal muscle-specific clusters. **C**) Biological process categories identified following GREAT annotation of satellite cell-specific loci. **D**) IGV track displaying chromatin accessibility at *CALCR* and *EDN3* loci in freshly-isolated satellite cells and other tissues. Loci identified

specifically in freshly-isolated satellite cells, myoblasts and skeletal muscle are reported below the ATAC-seq tracks. RNA expression levels in freshly-isolated satellite cells and cultured myoblasts are also indicated. Dashed black squares indicate satellite cell-specific loci.

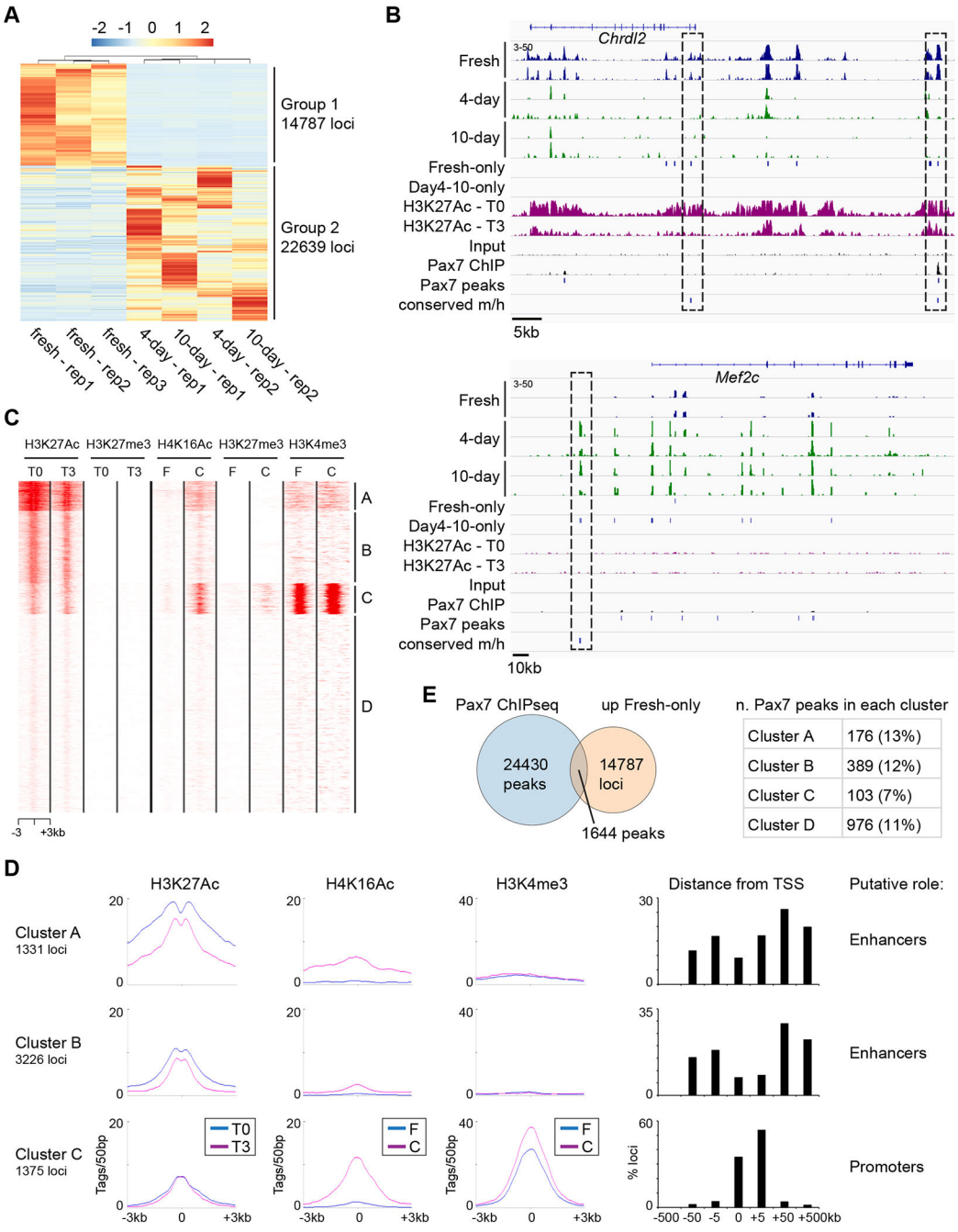

Fig. 3.

Chromatin accessibility profiling identifies enhancers in murine satellite cells. **A**) Heatmap displaying the differential accessible loci between freshly-isolated murine satellite cells (3 independent subsets), 4-day (2 independent subsets) and 10-day cultured cells (2 independent subsets). 4-day and 10-day cultured cells represent myoblasts. Group 1 and 2 indicate loci characterized by loss and gain of accessibility during the transition from freshly-isolated (activated) satellite cells and cultured myoblasts, respectively. **B)** IGV track displaying chromatin accessibility at *Chrdl2* and *Mef2c* loci in murine freshly-isolated

satellite cells (fresh) and myoblasts (cultured). H3K27Ac tracks report the deposition of this histone mark in *in situ* fixed (T0) and 3-hour post-isolation fixed (T3) satellite cells, representing quiescent and activated satellite cells. Pax7 genomic occupancy in ES-derived myogenic progenitors, detected Pax7 peaks and conserved differential accessible loci between murine and human datasets are indicated. Dashed black squares indicate differential accessible loci (reported in the Fresh-only and Cultured-only tracks). **C**) k-means clustering of H3K27Ac and H3K27me3 ChIP-seq data from T0 and T3 murine satellite cells, and H4K16Ac, H3K27me3 and H3K4me3 ChIP-seq data from freshly-isolated (F) and cultured (C) murine satellite cells. Mapped ChIP-seq data were used to generate a Density Tag Map centered on 14,787 up-Fresh ATAC-seq mouse peaks ± 3 kb. Cluster A: 1,331 loci; Cluster B: 3,226 loci; Cluster C: 1,375 peaks; Cluster D: 8,855 peaks. **D**) Distribution of H3K27Ac, H4K16Ac and H3K4me3 ChIP-seq reads across the ATAC-seq peak center ± 3 kb for Clusters A, B and C shown in panel C. Distance from TSS of the loci within each cluster and predicted function are reported on the right side. **E**) Schematic table reporting the number of Pax7 peaks overlapping to loci in Clusters A to D from panel C.

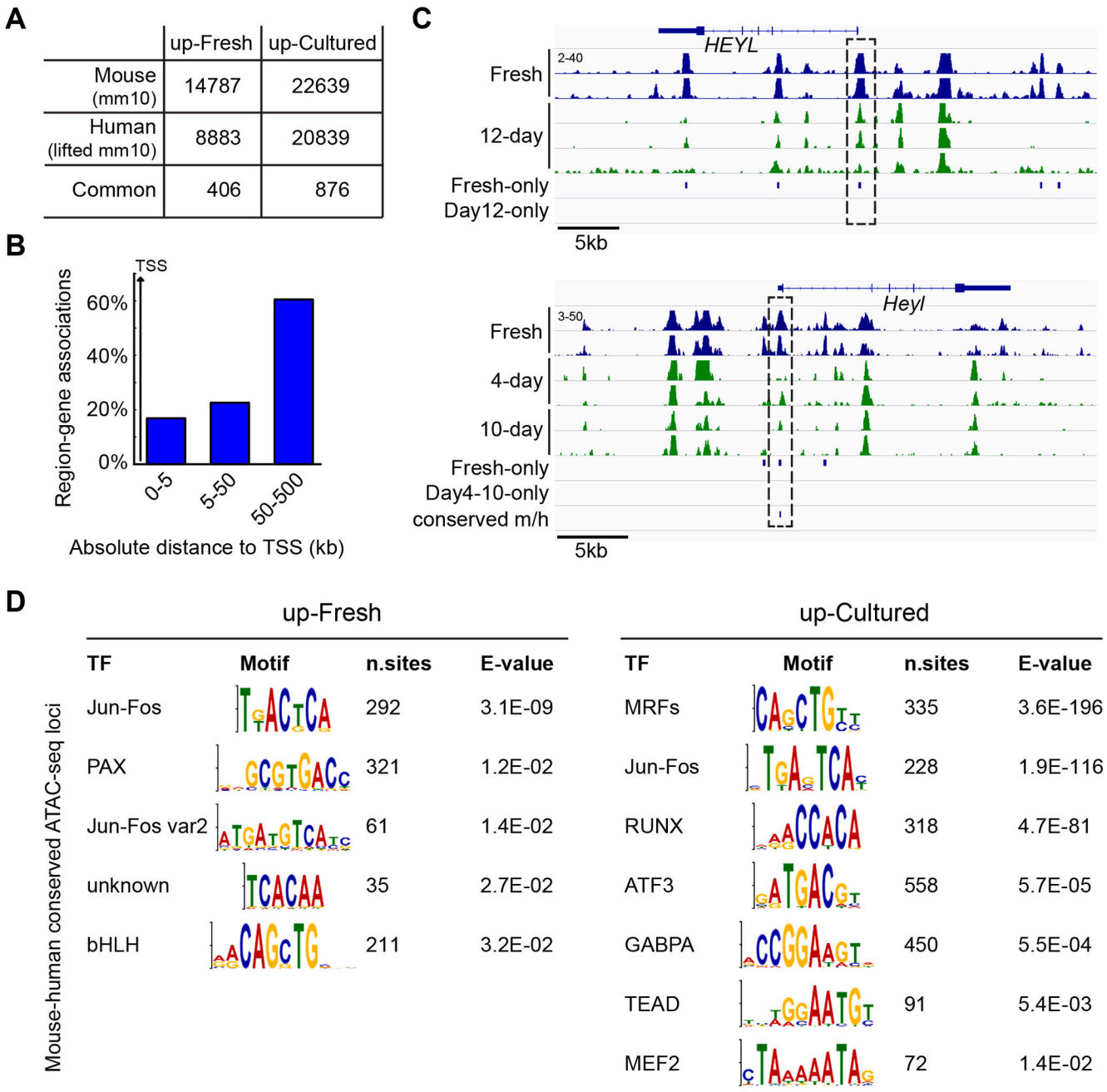

Fig. 4.

Conservation of chromatin accessible elements between human and murine activated satellite cells. **A**) Schematic table reporting the number of conserved human-mouse loci in up-Fresh and up-Cultured satellite cells. For this analysis, human coordinates were converted to the mm10 genomic coordinates. **B**) Genomic annotation of conserved Fresh-only loci. Distance from TSS is expressed in kilobases (kb). **C**) IGV track displaying chromatin accessibility at human and murine loci encoding for the NOTCH effector *HEYL* (*Heyl* for mouse) in freshly-isolated satellite cells (fresh) and myoblasts (cultured). Dashed black squares indicate conserved differential accessible loci. Conserved human-mouse loci

are indicated in the murine IGV track. **D**) Enriched transcription factor binding motifs (including number of motifs and E-value) identified in up-Fresh and up-Cultured conserved human-murine loci.

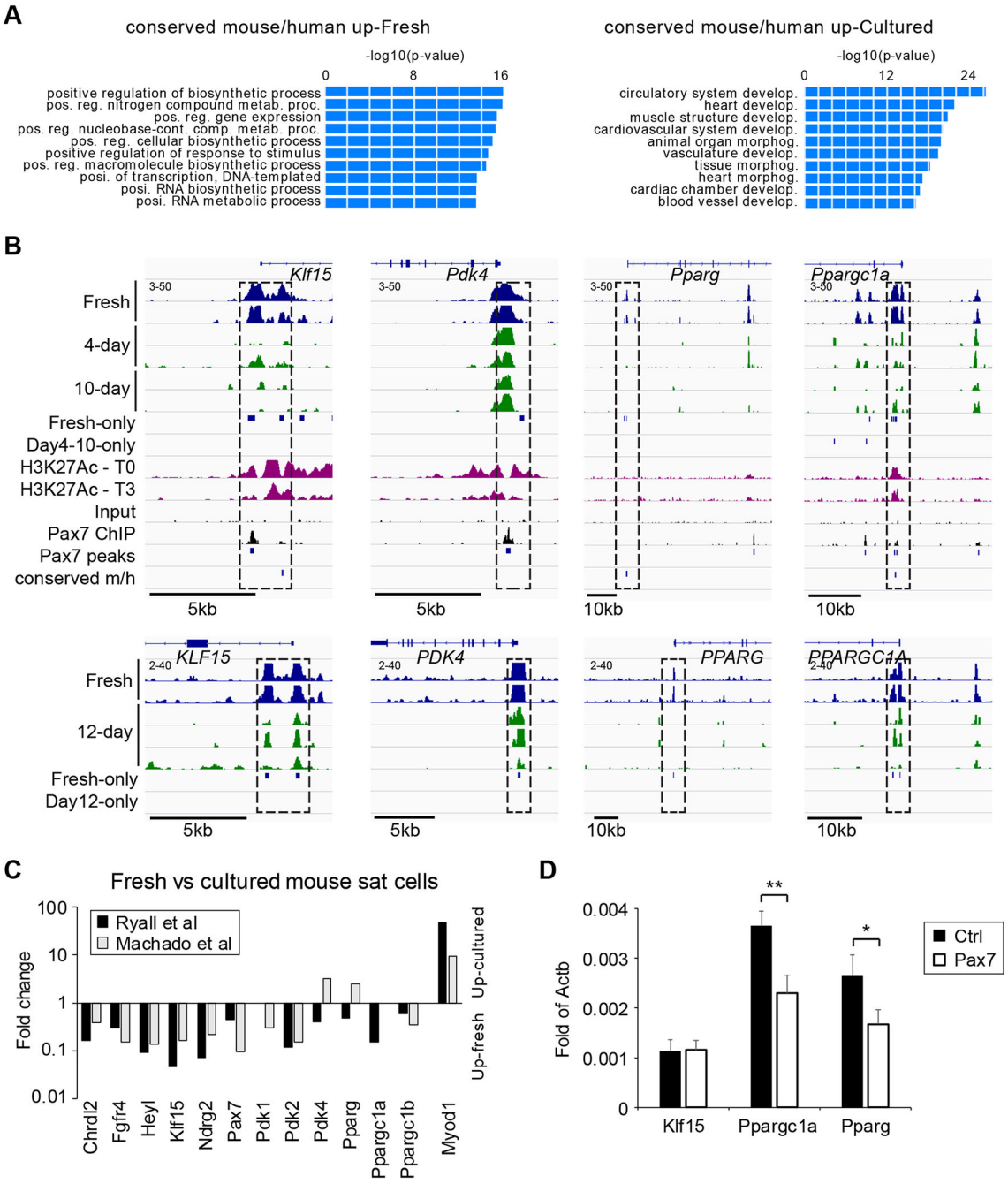

Fig. 5.

PPARGC1A and other metabolic regulator genes are potential Pax7 targets. **A**) Biological process categories identified following GREAT annotation of conserved human-mouse up-Fresh and up-Cultured loci. **B)** IGV track displaying chromatin accessibility at human and murine loci encoding for KLF15, PDK4, PPARG and PPARGC1A (*Klf15, Pdk4, Pparg* and *Ppargc1a* for mouse) in freshly-isolated satellite cells (fresh) and myoblasts (cultured). Dashed black squares indicate conserved differential accessible loci. Conserved human-mouse loci are indicated in the murine IGV track. **C**) Gene expression fold change

for selected genes (p-value < 0.05) from the comparisons quiescent-vs-activated (Machado et al) and activated-vs-cultured (Ryall et al) murine satellite cells. **D**) Gene expression analysis following Pax7 overexpression in cultured murine satellite cells. Graph represents mean + s.d. of n = 3 independent biological replicates. Student's *t*-test *p < 0.05, **p < 0.01.

Table 1

Basic demographic data of human subjects.

Deidentified id	Age (year)	Gender	In-person measured height (cm)	In-person measured weight (kg)	BMI
1	43.9	female	162 cm	60 kg	22.86
4	24.9	male	187 cm	78.8 kg	22.53
6	23.1	male	185 cm	72.6 kg	21.21
5	35.8	female	161.5 cm	83.9 kg	32.17

KEY RESOURCES TABLE

REAGENT or RESOURCE	SOURCE	IDENTIFIER
Antibodies		
Mouse monoclonal anti-Myosin Heavy Chain	Developmental Studies Hybridoma Bank	MF20
Mouse monoclonal anti-PAX7	Developmental Studies Hybridoma Bank	PAX7
APC-conjugated anti-human CD56 antibody	Biolegend	clone 5.1H11
PE-conjugated anti-human CD82 antibody	Biolegend	clone ASL-24
Bacterial and Virus Strains		
pRRL-PGK-GFP	Trono Lab Misc Plasmids - Addgene	Addgene #12252
pRRL-PGK-Pax7	This study	N/A
Biological Samples		
Healthy adult human muscle tissue	University of Minnesota	STUDY00002730
Chemicals, Peptides, and Recombinant Proteins		
Human Fc-block	Miltenyi Biotec	130-059-901
Dexamethasone	Cayman Chemical	11015
basic-FGF	Peprotech	100-18B-250mg
Chick embryonic extract	US Biologies	C3999
Tn5 transposase+modified transposon	Illumina	TruSeq kit
Deposited Data		
Raw and analyzed data	This paper	GEO: GSE165414
Experimental Models: Cell Lines		
HEK 293T cells	ATCC	CRL-3216
Experimental Models: Organisms/Strains		
Mouse: Tg *Pax7-ZsGreen*	Bosnakovski D et al, 2008	N/A
Oligonucleotides		
Ppargc1a (Mm01208835_m1)	Life Technologies	Cat#4453320
Pparg (Mm00440940_m1)	Life Technologies	Cat#4331182
Klf15 (Mm00517792_m1)	Life Technologies	Cat#4448892
Actb (Mm02619580_g1)	Life Technologies	Cat#4331182